

## Raman and birefringence studies of the low-temperature phase transitions in $\text{LiK}_{1-x}\text{Rb}_x\text{SO}_4$ crystals

R. L. Moreira, P. Bourson,\* U. A. Leitão, A. Righi, L. C. M. Belo, and M. A. Pimenta  
*Departamento de Física, Instituto de Ciências Exatas, Universidade Federal de Minas Gerais, C.P. 702,  
30161-970 Belo Horizonte, MG, Brazil*

(Received 16 May 1995)

The low-temperature phase transitions of  $\text{LiK}_{1-x}\text{Rb}_x\text{SO}_4$  mixed crystals have been studied by Raman spectroscopy ( $x=0.10$  and  $0.50$ ) and birefringence measurements ( $x=0.10, 0.20$ , and  $0.50$ ). The mixed compounds with low Rb concentration undergo the same sequence of low-temperature phase transitions as the pure compound  $\text{LiKSO}_4$ . The mixed crystals' Raman spectra are very similar to those of the pure compound, showing that the presence of the Rb ions introduces a local distortion without destroying the long-range order of the crystalline arrangement. In the mixed crystals, the hexagonal-trigonal phase transition is shifted to higher values of temperature and the ferroelastic transition to lower values, with increasing Rb concentration. A qualitative model, whose basic assumption is the local trigonal distortion introduced by the Rb ions, is proposed to explain the experimental results.

### I. INTRODUCTION

In spite of the similarity of their chemical formula, the double sulfates of the family  $\text{LiASO}_4$ , where  $A$  is an alkali cation (Li, Na, K, Rb, and Cs), exhibit absolutely different sequences of structural phase transitions. The differences are related to the number of phase transitions and the symmetries of the distinct structures. The existence of a number of different structures is closely related with the dynamics and the possible orientations of the sulfate tetrahedra groups in the structure.

The small cation compounds, like  $\text{Li}_2\text{SO}_4$  and  $\text{LiNaSO}_4$ , undergo a superionic phase transition at high temperature.<sup>1,2</sup> Above this phase transition their structures have cubic symmetries and are characterized by a complete rotational disorder of the sulfate anions, typical of plastic crystals.<sup>3,4</sup> At room temperature  $\text{Li}_2\text{SO}_4$  presents a monoclinic structure ( $P21/a$  space group) (Ref. 5) and  $\text{LiNaSO}_4$  has a trigonal symmetry structure belonging to the  $P31c$  space group.<sup>6</sup> To our knowledge, there is no report of any structural phase transition of these compounds below room temperature.

Lithium potassium sulfate ( $\text{LiKSO}_4$ ) is, by far, the most interesting crystal of this family. It undergoes several phase transitions at high and low temperatures (the exact number of phase transitions is still an open question).<sup>7-13</sup> The highest temperature phase (above 943 K) has a hexagonal symmetry ( $P6_3/mmc$ ) (Ref. 14) and is also characterized by a rotational disorder of the sulfate anions which is associated with the mobility of the cations (certainly not comparable with  $\text{Li}_2\text{SO}_4$  and  $\text{LiNaSO}_4$ , but high enough to consider it as a superionic). By cooling the crystal, the *rotational* disorder of the sulfate ions (and the ionic conductivity) decreases by steps and finally it disappears at about 708 K, yielding another hexagonal structure ( $P6_3$  space group) (Ref. 15) which

is stable at room temperature. Between these two hexagonal phases there is an intermediate phase ( $943 < T < 708$  K) with a symmetry certainly lower than hexagonal. A modulated structure (commensurate and incommensurate) has been proposed for this intermediate phase.<sup>16</sup>

It is important to emphasize that the dynamics in the orientation of the sulfate groups persists until low temperatures. That is, at room temperature, the sulfate groups are no more free to rotate, but their apex point dynamically into three equivalent directions related by a threefold symmetry around the hexagonal  $c$  axis. The gradual freezing of the *orientational* disorder and the accommodation of the sulfate in different orientations are responsible for the existence of other phase transitions at low temperature. At about 205 K the crystal undergoes a reconstructive phase transition (without group to subgroup relation), from the hexagonal  $P6_3$  room-temperature structure to a trigonal  $P31c$  symmetry structure.<sup>17,18</sup> Bansal and Roy<sup>18</sup> proposed that this phase transition is due to the reorientation of one sulfate group in each unit cell (in the hexagonal and trigonal structures, there are two formulae per unit cell). It was also observed the coexistence of these two different structures in a broad temperature range.<sup>19</sup>

Continuing the cooling process, the crystal undergoes a ferroelastic phase transition at about 190 K,<sup>20</sup> which is related to the freezing of the orientational disorder of the sulfate groups. Below this phase transition, all equivalent sulfate groups in a given macroscopic region of the crystal point in the same direction. Since there are three equivalent directions around the  $c$  axis, three kinds of ferroelastic domains related between each other by a threefold symmetry are generated.<sup>19</sup> The breakdown of the local threefold symmetry gives rise to a monoclinic structure, probably belonging to the group  $Cc$ .<sup>21</sup>

There are several experimental studies devoted to the very low-temperature phase transitions of  $\text{LiKSO}_4$ , but their results and interpretations are often contradictory in the litera-

ture. Certainly another phase transition occurs at about 35 K.<sup>22</sup> Conclusive results concerning the existence of phase transitions below 150 K and about the symmetries of the different structures are still lacking.

Lithium rubidium sulfate ( $\text{LiRbSO}_4$ ) in another member of this family which exhibits a very interesting sequence of phase transitions.<sup>23</sup> It is one of the rare sulfate compounds that certainly presents an incommensurate structure.<sup>24,25</sup> An interesting sequence of modulated structures occurs between 439 and 477 K, in which the wave vector of the modulation passes through an incommensurate ( $q/c^* = 2/5 - \delta$ ) and different commensurate values ( $q/c^* = \frac{3}{7}, \frac{1}{2},$  and  $\frac{2}{5}$ ). The room-temperature phase has a monoclinic  $P112_1/n$  symmetry.<sup>26</sup> There is no report in the literature claiming the existence of phase transitions below room temperature for this compound.

Surprisingly, lithium cesium sulfate ( $\text{LiCsSO}_4$ ) is a well-behaved crystal. According to the data reported in the literature, it undergoes only one phase transition at 202 K; and the low-temperature phase is ferroelastic.<sup>27,28</sup> The room-temperature structure has an orthorhombic  $Pm\bar{c}n$  symmetry while the ferroelastic phase belongs to the  $P112_1/n$  monoclinic space group.<sup>29,30</sup>

We are now studying systematically the mixed compounds of the type  $\text{LiK}_{1-x}\text{A}_x\text{SO}_4$ . The purpose of these studies is to investigate how the sequence of phase transitions of the pure compounds is affected by the random presence of cations of different sizes and to study the influence of the compositional disorder on the physical properties discussed above (ionic mobility, incommensurability, ferroelasticity, coexistence of different structures, etc.). In a previous work,<sup>31</sup> we have studied the high-temperature phase transitions of  $\text{LiK}_{1-x}\text{Na}_x\text{SO}_4$  crystals for  $x=0.10$  by means of electrical conductivity measurements. Results suggested the existence of clusters of the pure compounds mixed with the solid solution.

Single crystals of the type  $\text{LiK}_{1-x}\text{Rb}_x\text{SO}_4$  are very suitable for investigations since solid solutions are formed in the whole region of concentration  $x$ . Moreover, the pure compounds  $\text{LiKSO}_4$  and  $\text{LiRbSO}_4$  are the members of the family that present the most interesting sequences of phase transitions. These mixed compounds have been synthesized and investigated by means of different experimental techniques. The purpose of the present paper is to report on our low temperature Raman scattering and birefringence studies of  $\text{LiK}_{1-x}\text{Rb}_x\text{SO}_4$  crystals for  $x=0.10, 0.20,$  and  $0.50$ .

## II. EXPERIMENTAL DETAILS

Single crystals of  $\text{LiK}_{1-x}\text{Rb}_x\text{SO}_4$  have been grown at 313 K by means of slow evaporation of saturated aqueous solutions containing the salts  $\text{Li}_2\text{SO}_4\cdot\text{H}_2\text{O}$ ,  $\text{K}_2\text{SO}_4$ , and  $\text{Rb}_2\text{SO}_4$  in several molar ratios. X-ray fluorescence analysis confirmed that the concentration of the alkali cations found in the crystals was practically the same introduced in the aqueous solution. For  $x=0.10$ , we have obtained crystals of good optical quality with dimensions of about  $15\times 15\times 10$  mm<sup>3</sup>. For the other concentrations typical dimensions were much smaller. The samples have been cut from regions free of visible twinning and polished for optical measurements. The crystallographic axes have been indexed similarly to the

case of the pure compound  $\text{LiKSO}_4$ , that is,  $c$  is the hexagonal axis and  $a$  is perpendicular to  $c$  and parallel to a natural face of the crystal.

The Raman spectra were recorded with a DILOR XY micro-Raman triple monochromator equipped with a gold-array detector. The birefringence was measured using the Senarmont method, with a computer-controlled apparatus having an ultimate resolution of  $\delta(\Delta n) \leq 3 \times 10^{-8}$ . The mechanical pressure was measured using a homemade calibrated stress-gage system, having a resolution of  $\delta p = \pm 0.5$  bar and reproducibility of 1%. The stress-gage system was adapted to the cryostat, allowing the study of the uniaxial pressure dependence of  $\Delta n$  at low temperature. A gas flow cryostat was used to vary the temperature between 80 and 300 K, with an accuracy of about 0.01 K.

## III. GROUP THEORY ANALYSIS

In the mixed crystals of the type  $\text{LiK}_{1-x}\text{Rb}_x\text{SO}_4$  the rubidium ions replace the potassium ions and certainly introduce a local distortion in the structure. However, it will be shown in the analysis of the experimental data that these crystals experiment the same sequence of low-temperature phase transitions showed by the pure compound  $\text{LiKSO}_4$ . For low values of  $x$ , the mixed crystals present an average hexagonal symmetry ( $P6_3$  space group) at room temperature, and they undergo phase transitions at low temperature to a trigonal ( $P31c$  space group) and, further one, to a ferroelastic structure. Therefore, we will use the Group theory predictions of the vibrational spectra of  $\text{LiKSO}_4$  to analyze the Raman spectra of the  $\text{LiK}_{1-x}\text{Rb}_x\text{SO}_4$  crystals.

In the case of the hexagonal room-temperature structure (space group  $P6_3$ ), the Raman active modes are those belonging to the  $A$ ,  $E_1$ , and  $E_2$  irreducible representations. The  $A$  and  $E_1$  modes are polar and consequently the frequencies of the longitudinal components are shifted with respect to the transverse ones. The  $A$  modes are polarized in the  $z$  direction and the double degenerated  $E_1$  modes are polarized in the  $xy$  plane. The Raman active modes of the trigonal structure (space group  $P31c$ ) belong to the  $A_1$  and  $E$  irreducible representations and both are polar (the  $A_1$  modes in the  $z$  direction and the  $E$  modes in the  $xy$  plane). The structure of the ferroelastic phase has probably a monoclinic symmetry (space group  $Cc$ ) with four formulas per unit cell. All vibrational modes are Raman active and polar. In this case, the difficulty in the attribution of the mode symmetries in the Raman spectra arises from the existence of three kinds of ferroelastic domains, whose  $x$  and  $y$  directions are oriented at  $120^\circ$  with respect to each other. Since we have studied a multidomain sample in the Raman experiment, we will not discuss the selection rules predicted by group theory for this ferroelastic structure.

In our experiments we have used the scattering geometries  $z(xx)y$  and  $z(xy)y$ , following Porto's notation, which allow the investigation of the phonons propagating along the  $[0\bar{1}1]$  direction. For this direction of propagation, the long-range electrical forces associated to the polar modes mix the  $A$  and  $E_1$  symmetry modes.<sup>32</sup> Thus, we expect one pure transverse mode of  $E_1$  symmetry (polarized along the  $[100]$  direction) and two oblique polar modes with mixed symmetries. The degree of mixing symmetry of these polar modes

TABLE I. Raman-active modes for the hexagonal and trigonal  $\text{LiKSO}_4$  symmetries.

Attribution	$\rightarrow$	$\nu_1$	$\nu_2$	$\nu_3$	$\nu_4$	Ext	Lib	Number of Raman modes	Nonzero Raman tensor elements
Hexagonal	$A$	1	0	1	1	2	1	6	$xx, yy, zz$
$C_6(6)$	$E_1$	0	1	1	1	2	1	6	$xz, yz$
	$E_2$	0	1	1	1	3	1	7	$xx, yy, xy$
Trigonal	$A_1$	1	0	1	1	2	1	6	$xx, yy, zz$
$C_{3v}(3m)$	$E$	0	2	2	2	5	2	13	$xx, yy, xy, xz, yz$

depends whether the long-range electrical forces predominate or not over anisotropy in the short-range electrical forces, and this is a characteristic of each polar mode. Therefore, this oblique direction of propagation is expected to be very sensitive to small changes that occur at the phase transition temperatures. The nonpolar  $E_2$  modes are observed in the  $z(xx)y$  scattering geometry. It must be emphasized that the frequencies observed in our spectra are really very close to those observed in the pure compound  $\text{LiKSO}_4$  for scattering geometry which do not mix the irreducible representations associated to the polar modes. This result allows us to perform the mode attribution accordingly to the pure polarization states.

Table I shows the number and the attribution of the Raman-active modes belonging to each irreducible representation for the hexagonal and trigonal phases (considering the same unit cell of the pure compound  $\text{LiKSO}_4$ ), and the Raman tensor elements associated to each irreducible representation. The internal modes  $\nu_3$ ,  $\nu_1$ ,  $\nu_4$ , and  $\nu_2$  account, respectively, for the asymmetrical stretching, symmetrical stretching, asymmetrical bending, and symmetrical bending modes of the  $\text{SO}_4^{2-}$  tetrahedra.

#### IV. RESULTS AND DISCUSSIONS

##### A. Birefringence measurements

Birefringence measurements on  $\text{LiK}_{1-x}\text{Rb}_x\text{SO}_4$  system have been carried out under uniaxial pressure applied along the  $b$  axis ( $\sigma_{yy}$  of  $\sim 50$  bars), in order to induce a ferroelastic monodomain at low temperatures.<sup>33</sup> Figure 1 presents the temperature dependence of the out-of-plane birefringence for a sample with  $x=0.10$ ,  $\Delta n_{bc}(T) - \Delta n_{bc}(300\text{ K})$ , on the cooling (solid circles) and on the heating (open circles) runs. Measurements have been done after a large temperature cycle, the temperature being reversed at 80 K, and after a partial temperature cycle (crosses) where the reversing temperature was 190 K. These results appear to be quite similar to those showed by the pure  $\text{LiKSO}_4$  crystal, reported in a previous work.<sup>33</sup> We note two well defined anomalies at about 226 and 164 K in the cooling process (located at 278 and 168 K, on the heating curve) which we associate, as it will become clear with subsequent data, to the same sequence of phase transitions of the pure crystal, namely, hexagonal to trigonal and trigonal to ferroelastic transitions, respectively. In the hexagonal and trigonal phases, the temperature dependence of the out-of-plane birefringence is dominated by the small difference on the thermal expansion coefficients of the lattice parameters, which gives rise to the

almost linear temperature behavior observed in Fig. 1 (except for the anomaly at the hexagonal to trigonal transition, originated from the  $c$  lattice parameter jump at this transition). This is not the case in the ferroelastic phase, where the in-plane elastic deformation leads to an important change in the  $yy$  refraction index and so, in the  $\Delta n_{bc}$  birefringence.

When compared to the pure crystal, the present results show very similar thermal hysteresis (4 K for the ferroelastic phase transition and 52 K for the trigonal one). On the other hand, the transition temperatures are shifted in such a way that the temperature region where the trigonal phase exists has been enlarged. The ferroelastic phase becomes less stable with the addition of Rb ions, the converse holding for the trigonal phase, for which the upper transition temperatures increase.

By comparing the large and partial temperature cycles we perceive different signals into the trigonal phase, depending on the achieving or not the ferroelastic phase. Moreover, after heating the sample above the trigonal-to-hexagonal transition the birefringence signal drops down to the same values we observe at the start of the experiment, so that we cannot ascribe this effect as an extrinsic one. These facts are very surprising and are not observed in this magnitude in the pure crystal. They need to be further investigated to be fully understood.

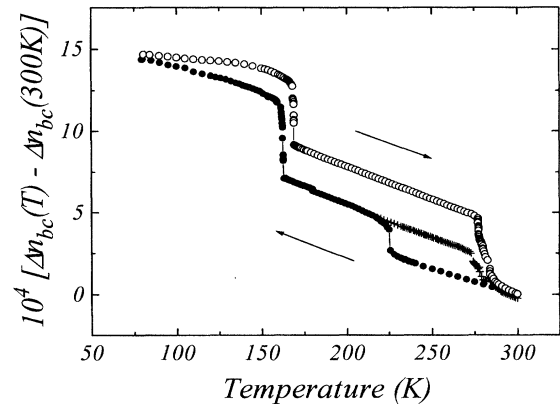


FIG. 1. Temperature dependence of the out-of-plane birefringence of an  $x=0.10$  mixed crystal,  $\Delta n_{bc}(T) - \Delta n_{bc}(300\text{ K})$ , under constant uniaxial pressure ( $\sigma_{yy} = 50$  bars), in the cooling (solid circles) and heating (open circles) processes, after a large temperature cycle, the temperature being reversed at 80 K. (The crosses show the heating data after a small temperature cycle, reversing temperature 190 K.)

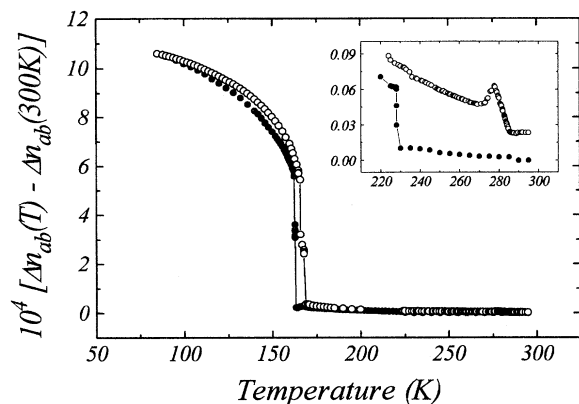


FIG. 2. Temperature dependence of the in-plane birefringence of an  $x=0.10$  mixed crystal,  $\Delta n_{ab}(T)$ , under constant uniaxial pressure ( $\sigma_{yy}=50$  bars), in the cooling (solid circles) and heating (open circles) processes. The inset shows the behavior of the in-plane birefringence in the vicinity of the hexagonal to trigonal transition.

Let us now study the in-plane birefringence temperature behavior of this crystal, presented in Fig. 2. In this figure solid and open circles represent, respectively, the cooling and heating measurements. The figure presents also an inset with a zoom around the trigonal transition. The present results are well compatible with those presented in Fig. 1, i.e., we observe two anomalies accompanying the phase transitions (at approximately the same temperatures) and the existence of thermal hysteresis. The very large in-plane birefringence into the ferroelastic phase originates directly from the elastic deformation. On the other hand, in-plane birefringence appears into the trigonal phase owing to the piezo-optic effect, since the measurements were taken under uniaxial pressure. We remark also that the in-plane birefringence values for this mixed crystal ( $x=0.10$ ) are very close to those of the  $\text{LiKSO}_4$  pure crystal—in particular, the birefringence jump at the ferroelastic transition.<sup>33</sup> This indicates that these two samples present similar elastic deformations at the ferroelastic phase.

We present now the birefringence results for a sample with  $x=0.20$ . Figure 3 shows the temperature changes of the out-of-plane birefringence for this crystal, on the cooling (solid circles) and on the heating (open circles) processes, after the large temperature cycle (the temperature being reversed at 80 K). We note first the presence of the strong anomaly associated to the hexagonal-to-trigonal phase transition on the otherwise almost linear curves. However, the anomaly associated with the ferroelastic transition is very faint, certainly due to the presence of ferroelastic domains. This assumption is verified also by the in-plane results, present in Fig. 4, for the same mixed crystal. In this figure, cooling (solid circles) and heating (open circles) runs show also the presence of not reproducible jumps and irreversibilities, which indicate the presence and the reorientation of ferroelastic domains. The attempts to induce monodomain state in these  $x=0.20$  mixed crystals by increasing the uniaxial pressure were not successful, since the samples crack before full monodomain formation, for  $\sigma_{yy}$  of  $\sim 150$  bars.

Although less pronounced, the birefringence anomalies for this  $x=0.20$  crystal present the same features as the pure

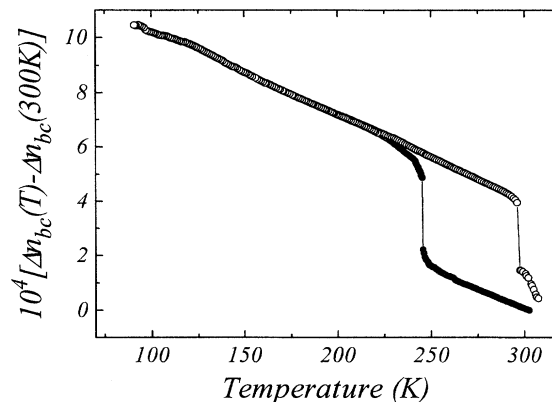


FIG. 3. Temperature dependence of the out-of-plane birefringence of an  $x=0.20$  mixed crystal,  $\Delta n_{bc}(T) - \Delta n_{bc}(300\text{ K})$ , under constant uniaxial pressure ( $\sigma_{yy}=50$  bars), in the cooling (solid circles) and heating (open circles) processes.

$\text{LiKSO}_4$  crystal, inducing us to conclude that these anomalies correspond to the same structural phase transition. We also observe that the transition temperatures are still more affected: 250 K for the hexagonal-trigonal transition and 134 K for the ferroelastic one, during the cooling process (302 and 144 K, for the same transitions, in the heating runs).

In order to clarify the transition temperature dependence with Rb ion contents, we present in Fig. 5 the observed low-temperature phase diagram for the  $\text{LiK}_{1-x}\text{Rb}_x\text{SO}_4$  system, for  $x$  ranging from 0 to 0.20. The results, except for the sample with  $x=0.15$  measured by differential scanning calorimetry, were taken from the averages of the critical temperatures denoted by the birefringence anomalies. In Fig. 5 the symbols  $T_\Delta$  and  $T_F$  represent, respectively, the hexagonal-trigonal and the ferroelastic transitions, in the heating (+) and cooling (−) processes. Note the enlarging of the region of existence of the trigonal phase and the positive (negative) slope for the curve corresponding to the hexagonal-trigonal (ferroelastic) transition with the increasing Rb concentration.

If we assume that the crystal with  $x=0.50$  presents the same symmetry phases as the  $\text{LiKSO}_4$  pure crystal, direct

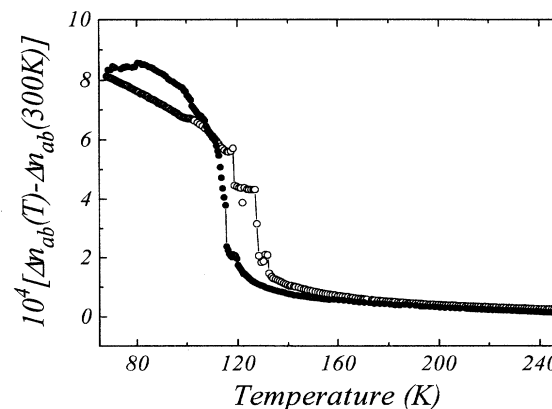


FIG. 4. Temperature dependence of the in-plane birefringence of an  $x=0.20$  mixed crystal,  $\Delta n_{ab}(T)$ , under constant uniaxial pressure ( $\sigma_{yy}=50$  bars), in the cooling (solid circles) and heating (open circles) processes.

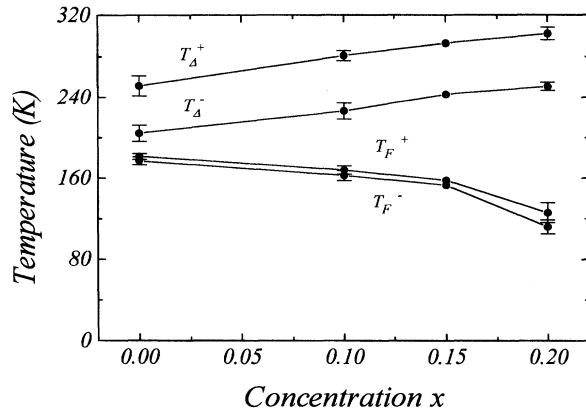


FIG. 5. Low-temperature phase diagram for the  $\text{LiK}_{1-x}\text{Rb}_x\text{SO}_4$  mixed crystals. The observed hexagonal-trigonal and ferroelastic critical temperatures are, respectively, represented by  $T_{\Delta}$  and  $T_F$ , for the cooling (–) and heating (+) runs.

extrapolation of data of Fig. 5 would give their transition temperatures out of the temperature range studied here. We have measured the temperature dependence of the out-of-plane birefringence for this crystal. The results are present in Fig. 6, where cooling and heating processes are represented, respectively, by solid and open symbols. In these curves, no anomaly has been detected. The well-behaved out-of-plane birefringence shows only the lattice thermal expansion, and presents a strong evidence against the existence of phase transitions between 80 and 300 K.

### B. Raman studies

Raman spectroscopy has been used to investigate the low-temperature phase transitions of the  $\text{LiK}_{1-x}\text{Rb}_x\text{SO}_4$  system and to give information about the symmetries of the low-temperature phases. In fact, many authors have used this technique to study the low-temperature phase transitions of the  $\text{LiKSO}_4$  pure crystal, presenting the vibrational mode assignment for the hexagonal and trigonal phases.<sup>17,18,22,34–36</sup> We use these data to characterize our mixed crystals. At

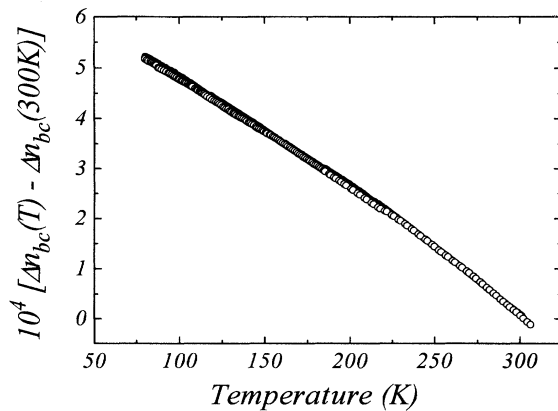


FIG. 6. Temperature dependence of the out-of-plane birefringence of an  $x=0.50$  mixed crystal,  $\Delta n_{bc}(T) - \Delta n_{bc}(300\text{K})$ , under constant uniaxial pressure ( $\sigma_{yy} = 50$  bars), in the cooling (solid) and heating (open circles) processes.

room temperature, the as-grown  $x=0.10$  and  $0.20$  crystals present the same bands as the pure  $\text{LiKSO}_4$  crystal, while the crystal with  $x=0.50$  presents different spectra. It is interesting to observe that the band linewidths of the mixed compounds are practically the same as in the pure compound.

Let us now analyze the temperature changes of the spectra for the different concentrations. Figure 7 exemplifies the changes in the spectra during the cooling of the crystal with  $x=0.10$ , in the  $z(xx)y$  configuration, in two spectral regions: (a)  $320\text{--}580\text{ cm}^{-1}$  (external modes associated to the lithium ions and the  $\nu_2$  symmetric  $\text{SO}_4^{2-}$  bending modes) and (b)  $580\text{--}680\text{ cm}^{-1}$  ( $\nu_4$  asymmetric  $\text{SO}_4^{2-}$  bending modes). The observed spectral evolutions (in particular, the appearance of new Raman bands) are very similar to those presented by the pure  $\text{LiKSO}_4$  crystal for the same spectral regions and configuration, and present a first evidence for the proposed hexagonal-trigonal and ferroelastic transitions for this mixed crystal. In order to analyze the detailed changes in the Raman spectra, we present schematically in Figs. 8 and 9 the temperature evolution of the frequencies of the most intense peaks of the  $x=0.10$  mixed crystal, during the cooling process.

Figure 8 shows the temperature evolution of the Raman frequencies of two external ( $410$  and  $443\text{ cm}^{-1}$ ), and two internal ( $\nu_2$  at  $467\text{ cm}^{-1}$  and  $\nu_4$  at  $635\text{ cm}^{-1}$ ) modes in the  $z(xz)y$  configuration. The external modes are well behaved, presenting only a small shift to higher frequencies on cooling the material, which is a general case in this family of compounds (except for some few details which will be discussed later). Nevertheless, we note that, below  $160\text{ K}$ , the frequency shift of the  $410\text{ cm}^{-1}$  external mode is more important than for the other modes. The variations of the internal bending modes are more interesting: the symmetrical mode splits at about  $155\text{ K}$ , while the asymmetrical one evolves slowly to three bands at low temperatures. These results are very similar to that of the pure crystal: the only difference is the signature of the  $626\text{ cm}^{-1}$  band above the characterized ferroelastic transition, since this band should appear only in the ferroelastic phase.

Figure 9 shows the temperature dependence of the Raman vibrational modes in the regions (a)  $20\text{--}500\text{ cm}^{-1}$  and (b)  $620\text{--}1250\text{ cm}^{-1}$ , in the  $z(xx)y$  configuration, for the same mixed crystal, during the cooling process. In this case, the spectra evolutions are also very similar to those of the  $\text{LiKSO}_4$  pure crystal. In particular, the hexagonal to trigonal transition is assigned by the splitting of two bands: the librational  $E_2$  mode located at  $56\text{ cm}^{-1}$  and the  $\nu_4$  mode ( $636\text{ cm}^{-1}$ ) and by the appearance of a new band located at about  $443\text{ cm}^{-1}$  [this band is originally the  $E_1(\text{LO})$  mode of the hexagonal phase. In the trigonal phase, this mode belongs to the  $E$  irreducible representation, thus it can be seen in both  $z(xx)y$  and  $z(xz)y$  configurations]. An additional very low-frequency band (near  $32\text{ cm}^{-1}$ ), which should be linked to a Rb translational mode, shows also a doubling near  $200\text{ K}$ .

Another interesting feature of the hexagonal to trigonal transition is the relative intensity changes of the  $\nu_3$  asymmetrical stretching bands in the  $z(xx)y$  configuration, presented in Fig. 10, for the cooling process. In the trigonal phase, the mode at  $1200\text{ cm}^{-1}$  becomes more intense than the other bands ( $1116$  and  $1120\text{ cm}^{-1}$ ). This behavior is

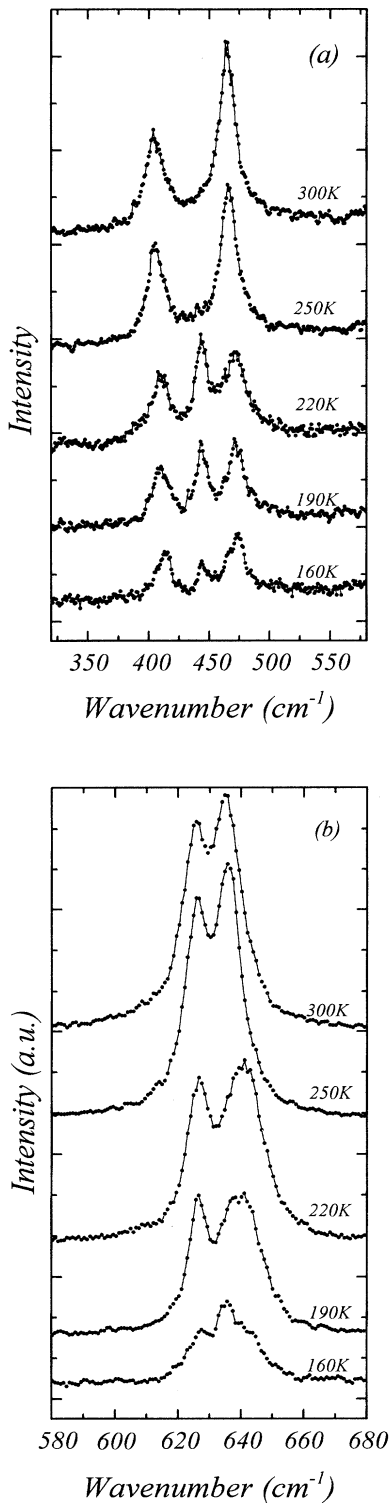


FIG. 7. Temperature dependence of the Raman spectra of an  $x=0.10$  mixed crystal, in the  $z(xx)y$  configuration, in two spectral regions: (a)  $320\text{--}580\text{ cm}^{-1}$  (external and  $\nu_2$  symmetric bending modes) and (b)  $580\text{--}680\text{ cm}^{-1}$  ( $\nu_4$  asymmetric bending modes), showing the changes accompanying the two phase transitions in the cooling process.

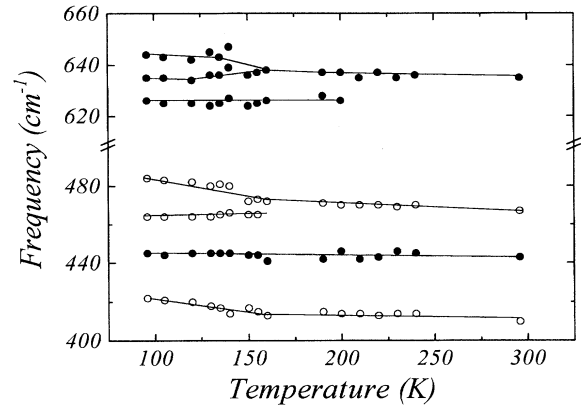


FIG. 8. Temperature dependence of the most intense low-frequency Raman modes, in the  $z(xz)y$  configuration, for the  $x=0.10$  mixed crystal, during the cooling process.

nearly the same for both mixed ( $x=0.10$ ) and pure crystals. The transition temperatures agree well with those observed in the birefringence measurements. The decrease of the relative intensity of this band on further cooling is due to the intensification of the  $1116\text{ cm}^{-1}$  band in the ferroelastic phase.

The ferroelastic transition is assigned by the doubling of the  $471\text{ cm}^{-1}$  band ( $\nu_2$ ) and by the intensity increasing of two bands:  $\nu_4$  ( $633\text{ cm}^{-1}$ ) and  $\nu_3$  ( $1116\text{ cm}^{-1}$ ) modes, occurring at about  $160\text{ K}$ . The latest mode was already present at higher temperatures but its intensity was too weak to be resolved in the spectra, due to the proximity with the  $1120\text{ cm}^{-1}$  band. Its enhancing into the ferroelastic phase (where it becomes stronger than the  $1120\text{ cm}^{-1}$  band) is also observed in the pure crystal. The other results are also similar for the two crystals, except that the pure crystal shows four  $\nu_4$  modes (instead of three showed by the  $x=0.10$  crystal). The fourth peak is originated by the doubling of the  $643\text{ cm}^{-1}$  of the pure crystal in two bands located at approximately  $647$  and  $638\text{ cm}^{-1}$ . In the mixed crystal we observe that the intensity of the mode of  $643\text{ cm}^{-1}$  decreases in the ferroelastic transition, while that of the  $633\text{ cm}^{-1}$  band increases, which shows simply that the missing mode is in fact superimposed to the latest band.

The data of Fig. 9(a) show also two other important features. First, the external hexagonal  $E_2$  mode at about  $409\text{ cm}^{-1}$  splits in two bands ( $406$  and  $412\text{ cm}^{-1}$ ) around  $210\text{ K}$ . The emerging band ( $412\text{ cm}^{-1}$ ) is not expected in the trigonal phase (in the pure crystal it appears only in the ferroelastic phase) and is in fact very weak. This band becomes intense in the subsequent transition for the ferroelastic phase. Second, we also note the doubling of the external mode around  $443\text{ cm}^{-1}$  below  $115\text{ K}$ , which is just accompanied by a small relative increase of the intensity of two other external modes ( $105$  and  $130\text{ cm}^{-1}$ ). The origin of the latest evolution is not understood but we remember that Oliveira *et al.*<sup>22</sup> have observed that some bands of the pure crystal located around  $500\text{ cm}^{-1}$  split below  $100\text{ K}$ .

Let us now present the Raman results for the crystal with  $x=0.50$ . We have observed that its room-temperature spectra are very similar to those of the trigonal phase of the  $\text{LiKSO}_4$  pure crystal. This result is shown for a chosen spec-

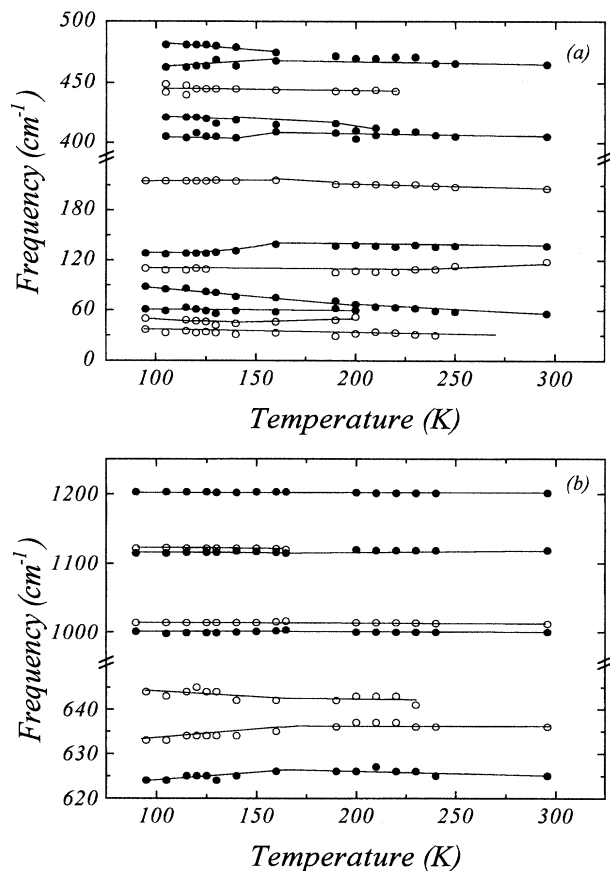


FIG. 9. Temperature dependence of the Raman vibrational modes in the region 20–500  $\text{cm}^{-1}$  (a) and 620–1250  $\text{cm}^{-1}$  (b), in the  $z(xx)y$  configuration, for the  $x=0.10$  mixed crystal, during the cooling process.

tral range (350–680  $\text{cm}^{-1}$ ) in Fig. 11. This figure presents the room-temperature spectra of three samples:  $x=0.50$  mixed crystal, pure  $\text{LiKSO}_4$  ( $x=0$ ), and  $\text{LiRbSO}_4$  crystals ( $x=1$ ), besides two characteristic low-temperature  $\text{LiKSO}_4$

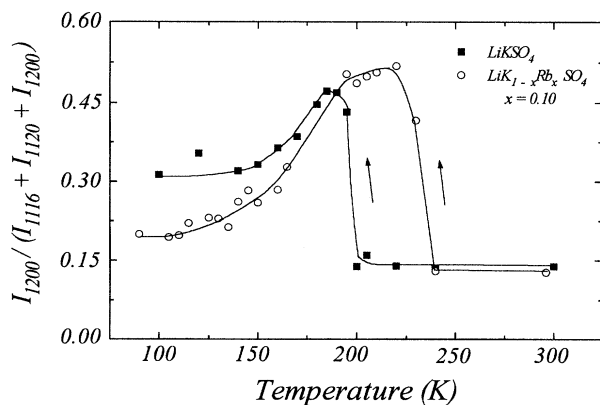


FIG. 10. Temperature dependence of the relative intensity of the  $\nu_3$  longitudinal mode taken into account the integrated intensities of the three asymmetrical stretching modes in the  $z(xx)y$  configuration, for pure  $\text{LiKSO}_4$  and the  $x=0.10$  mixed crystal, during the cooling processes.

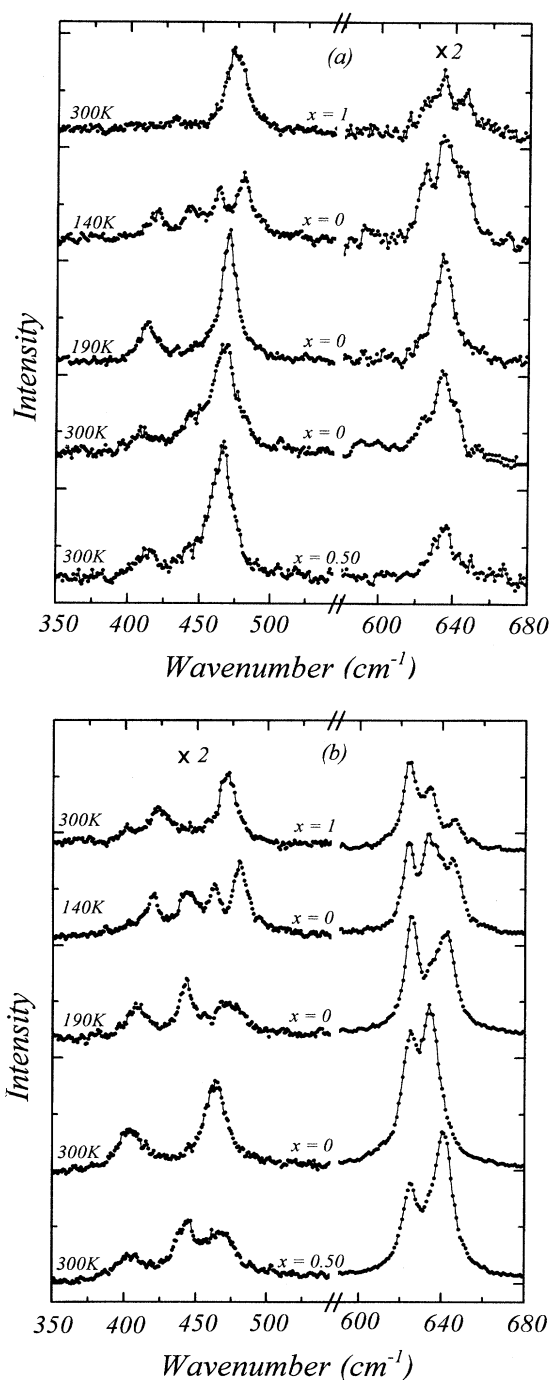


FIG. 11. Raman spectra in the region of the higher-frequency external modes and of the  $\nu_2$  and  $\nu_4$  internal modes for an  $x=0.50$  mixed crystal and for  $\text{LiKSO}_4$  ( $x=0$ ) and  $\text{LiRbSO}_4$  ( $x=1$ ) pure crystals, in  $z(xz)y$  (a) and  $z(xx)y$  (b) configurations. For the  $\text{LiKSO}_4$  sample, vibrational modes are indicated for the hexagonal (300 K), trigonal (190 K), and monoclinic (140 K) phases. For the other samples the spectra are taken at room temperature (300 K).

spectra in its trigonal (190 K) and monoclinic (140 K) phases, for both (a)  $z(xz)y$  and (b)  $z(xx)y$  configurations. The above-mentioned similarities between the spectra of the  $x=0.50$  sample and those of the trigonal phase of the

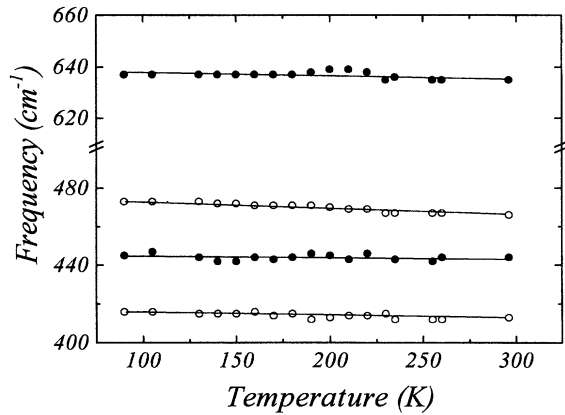


FIG. 12. Temperature dependence of the most intense low-frequency Raman modes, in the  $z(xz)y$  configuration, for the  $x=0.50$  mixed crystal, during the cooling process.

$\text{LiKSO}_4$  pure crystal are clearly seen by the comparison of the overall peak profiles. The same behavior is also observed for the other spectral ranges. In particular, the mixed crystal presents an intense band at  $1200\text{ cm}^{-1}$  in the  $z(xx)y$  geometry (absent in the pure  $\text{LiRbSO}_4$  crystal),<sup>37,38</sup> which is stronger than the other asymmetrical stretching modes ( $1116$  and  $1120\text{ cm}^{-1}$ ). As already noticed, this is a characteristic of the  $\text{LiKSO}_4$  trigonal phase.

We have investigated the temperature dependence of the Raman modes for this  $x=0.50$  sample. Figure 12 shows a quite normal temperature behavior of the two higher frequency external modes and the  $\nu_2$  and  $\nu_4$  modes, in the  $z(xz)y$  configuration, during the cooling process. These modes are well compatible with those of  $\text{LiKSO}_4$  in its trigonal phase.

The results for the  $z(xx)y$  configuration are presented in Fig. 13 ( $20\text{--}650\text{ cm}^{-1}$ ). The measurements were taken during the cooling process, between  $296$  and  $80\text{ K}$ . We note first the well-behaved temperature dependence of the Raman peak frequencies. A direct comparison of Figs. 13 and 9 [(a) and (b)], the latest one corresponding to the  $x=0.10$  mixed crystal, confirms the trigonal symmetry for the  $x=0.50$  sample in the whole temperature interval investigated. The only noticeable differences in the spectra presented by this crystal are: the absence of the  $110\text{ cm}^{-1}$  external mode in the whole temperature region investigated and an abnormal intensity change of two bands in the range  $225\text{--}210\text{ K}$  ( $443\text{ cm}^{-1}$  external mode and  $642\text{ cm}^{-1}$   $\nu_4$  mode), where their intensities are approximately a half of the values found outside this temperature interval.

## V. CONCLUSIONS

In the present work we have studied the low-temperature phase transitions of  $\text{LiK}_{1-x}\text{Rb}_x\text{SO}_4$  mixed crystals by means of Raman scattering ( $x=0.10$  and  $0.50$ ) and birefringence measurements ( $x=0.10$ ,  $0.20$ , and  $0.50$ ). We have observed that the low Rb concentration mixed crystals undergo the same sequence of low-temperature phase transitions as the

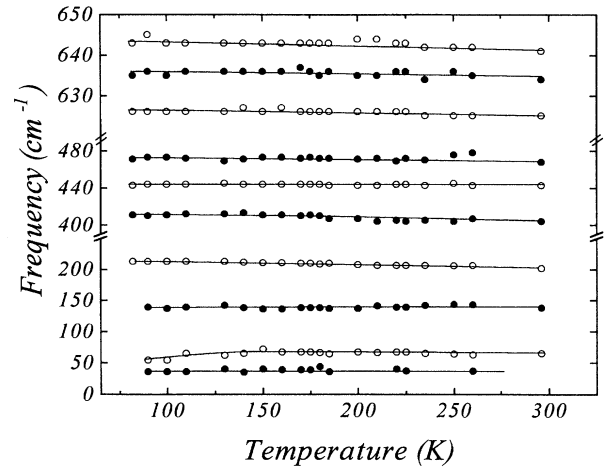


FIG. 13. Temperature dependence of the Raman vibrational modes between  $20$  and  $650\text{ cm}^{-1}$ , in the  $z(xx)y$  configuration, for the  $x=0.50$  mixed crystal, during the cooling process.

pure compound  $\text{LiKSO}_4$ , that is, from the hexagonal room temperature phase to a trigonal phase and at lower temperatures to a ferroelastic structure.

The Raman spectra of the mixed crystals are very similar to those of the pure compound, with exception of the appearance of a band at about  $32\text{ cm}^{-1}$  which is ascribed to vibrations involving the rubidium ion. We have observed the same number of Raman bands and their linewidths are comparable with those of  $\text{LiKSO}_4$  crystals. These results suggest that the presence of the rubidium ions at the potassium sites introduces a local distortion of the structure without destroying the long-range order of the crystalline arrangement.

It is interesting to observe that the introduction of the rubidium ion shifts the hexagonal-trigonal phase transition to higher values of temperature, and the ferroelastic phase transition temperature to lower values. In the concentration region  $x \leq 0.15$ , both the critical temperatures vary linearly with the rubidium concentration  $x$  and the slopes of the straight lines are  $2.65\text{ K}/\%\text{Rb}$  for the hexagonal-trigonal phase transition and  $-1.55\text{ K}/\%\text{Rb}$  for the ferroelastic transition. It is also interesting to observe that the value of the uniaxial pressure needed to generate a ferroelastic monodomain increases with the rubidium concentration  $x$ . For the  $x=0.20$  mixed crystals, the samples cracked before achieving a monodomain state.

In the case of the  $x=0.50$  compound, the Raman and birefringence studies showed the inexistence of phase transition between  $80$  and  $300\text{ K}$ . The extrapolation of the critical temperatures vs Rb concentration displayed in Fig. 5 suggests that, if these transitions exist in the  $x=0.50$  compound, they would be out of the temperature range investigated. Our results present strong evidences that the  $x=0.50$  mixed compound has a trigonal symmetry at room temperature.

Let us now present a simple model which tries to explain qualitatively the results discussed above. The basic assumption of this model is that the substitutional Rb ion occupies a greater volume in the unit cell than the K ion, due to its greater ionic radius ( $r_{\text{Rb}^+} = 1.52\text{ \AA}$  while  $r_{\text{K}^+} = 1.38\text{ \AA}$ ). This



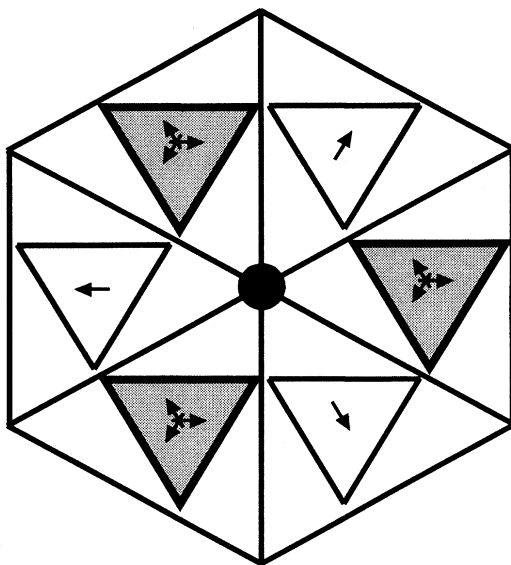


FIG. 14. Trigonal distortion induced by the presence of the substitutonal Rb ion. The three sulfate tetrahedra (open triangles), whose apex oxygens are in the same plane as the Rb ion, tilt in such a way that these oxygens withdraw itself radially, (see arrows).

is achieved into the ferroelastic phase by the repulsion of the oxygen atoms localized at the apex of the sulfate tetrahedra, which have the same  $z$  coordinate of the rubidium site. This situation is illustrated in Fig. 14. The repulsion of the apex oxygens results in a tilt of the three sulfate tetrahedra that are the nearest neighbors of the Rb ion (represented by white triangles in Fig. 14). Note that each one of these tetrahedra tilts around a different axis lying in the basal plane. Furthermore note that the other three tetrahedra are not affected by the presence of the Rb ion in first approximation (shadow triangles). As we have emphasized in the Introduction, the ferroelastic phase transition is accompanied by a collective tilting of all equivalent sulfate groups around the same axis lying in the basal plane. Thus, we can conclude that the presence of the rubidium ions plays against the ferroelastic transition by inhibiting the symmetry breaking associated to the ferroelastic phase transition. Since this phase transition is related to the freezing of the sulfate orientational disorder, it must occur at lower temperature for the mixed compounds.

Figure 14 shows also that the local distortion of the structure introduced by the Rb ion has a threefold symmetry. The ferroelastic transition occurs exactly by the breaking of the trigonal symmetry. Thus, the position occupied by the Rb ion becomes a center to where converge the domain walls. This situation is illustrated in Fig. 15, where a possible domain-wall configuration is presented. It is reasonable to suppose that the sizes of the ferroelastic domains decrease with increasing Rb concentration, since the Rb ions act as domain nucleation centers. This explains why it is more difficult to induce a ferroelastic monodomain in the mixed compounds. We remember that it was not possible to generate a monodomain in the  $x=0.20$  sample.

Figure 5 shows that the ferroelastic critical temperature vs Rb concentration curve leaves the linear behavior for

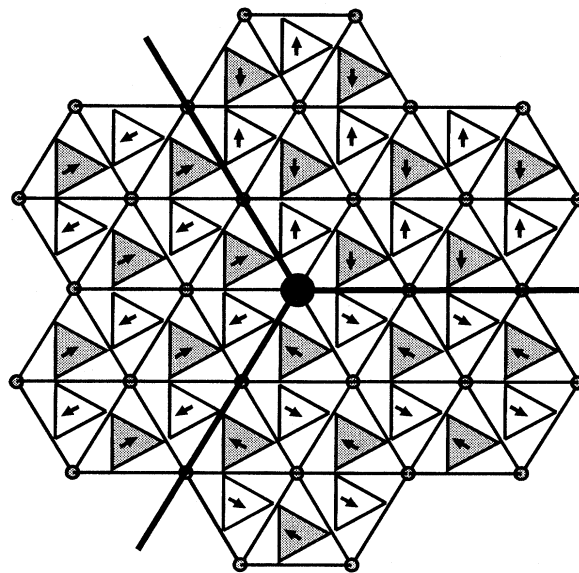


FIG. 15. The domain walls (bold lines) of the ferroelastic phase converge to the position occupied by the Rb ion. Small arrows indicate the dislocation of the apex oxygens.

$x > 0.15$ , i.e., in this region the ferroelastic transition temperature decreases faster with increasing  $x$ . For the  $x=0.50$  compound, we did not observe the ferroelastic transition. We made a conjecture that the percolation of the rubidium sites prevents the long-range order of the ferroelastic structure, thus inhibiting this phase transition.

Let us now discuss the effect of the Rb ions over the hexagonal-trigonal structure. In this case we suppose that it is simply related to the volume of the unit cell. As discussed in the Introduction, this phase transition is related to the re-orientation of one sulfate group in each unit cell. It is accompanied by the increase of the  $c$  lattice parameter with no change in the  $a$  lattice parameter, yielding a trigonal unit cell greater than the hexagonal one.<sup>39</sup> Since the rubidium ion occupies a greater volume in the unit cell, it certainly favors the trigonal structure. Its presence at low concentrations shifts the hexagonal-trigonal phase transition to higher values of temperature. For  $x > 0.20$ , the presence of the rubidium ions stabilizes the trigonal structure at room temperature.

A last remark concerns the concentration range  $x > 0.50$ , which we did not investigate in the present work. We remember that the pure compound  $\text{LiRbSO}_4$  has monoclinic structure at room temperature. It will be very interesting to investigate the phase diagram of the  $\text{LiK}_{1-x}\text{Rb}_x\text{SO}_4$  mixed crystals for  $0.50 < x < 1$  to see how these crystals behave in the presence of different structural tendencies.

#### ACKNOWLEDGMENTS

We thank our colleagues Dr. L. O. Ladeira for his help in the crystal growth and Dr. N. L. Speziali for the DSC data. This work was partially supported by the Brazilian agencies FINEP, FAPEMIG, and CNPq.

- \*Permanent address: Laboratoire MOPS-CLOES, SUPELEC, Université de Metz, 2, rue E. Belin, 57078 Metz cedex 3, France.
- <sup>1</sup>B. Heed, A. Lunden, and K. Schroeder, *Electrochim. Acta* **22**, 705 (1977).
- <sup>2</sup>A. F. Polishchuk and T. M. Shurzal, *ElektroKhimiya* **9**, 838 (1973).
- <sup>3</sup>L. Nilsson, J. O. Thomas, and B. C. Tofield, *J. Phys. C* **13**, 6441 (1980).
- <sup>4</sup>T. Förland, *Acta Crystallogr.* **11**, 224 (1958).
- <sup>5</sup>A. G. Nord, *Acta Crystallogr. B* **32**, 982 (1976).
- <sup>6</sup>B. Morosin and D. L. Smith, *Acta Crystallogr.* **22**, 906 (1967).
- <sup>7</sup>N. Choudhury, S. L. Chaplot, and K. R. Rao, *Phys. Rev. B* **33**, 8607 (1986).
- <sup>8</sup>R. Cach, P. E. Tomaszewski, and J. Bornarel, *J. Phys. C* **18**, 915 (1985).
- <sup>9</sup>M. Drozdowski and F. Holuj, *Ferroelectrics* **77**, 47 (1988).
- <sup>10</sup>H. Kabelka and G. Kuchler, *Ferroelectrics* **88**, 93 (1988).
- <sup>11</sup>H. Bill, Y. Ravi Sekhar, and D. Lovy, *J. Phys. C* **21**, 2795 (1988).
- <sup>12</sup>P. E. Tomaszewski and K. Lukaszewicz, *Phys. Status Solidi A* **71**, K53 (1982).
- <sup>13</sup>B. Mróz, J. A. Tuszynski, H. Kiefte, and M. J. Clouter, *J. Phys.: Condens. Matter* **1**, 5965 (1989).
- <sup>14</sup>Y. Y. Li, *Solid State Commun.* **51**, 355 (1984).
- <sup>15</sup>A. J. Bradley, *Philos. Mag.* **49**, 1225 (1925).
- <sup>16</sup>M. A. Pimenta, P. Echegut, Y. Luspín, G. Hauret, F. Gervais, P. Abélard, *Phys. Rev. B* **39**, 3361 (1989).
- <sup>17</sup>M. L. Bansal, S. K. Deb, A. P. Roy, and V. C. Sahni, *Solid State Commun.* **36**, 1047 (1980).
- <sup>18</sup>M. L. Bansal and A. P. Roy, *Phys. Rev. B* **30**, 7307 (1984).
- <sup>19</sup>G. J. Perpétuo, M. S. S. Dantas, R. Gazzinelli, and M. A. Pimenta, *Phys. Rev. B* **45**, 5163 (1992).
- <sup>20</sup>T. Breczewski, T. Krajewski, and B. Mróz, *Ferroelectrics* **33**, 9 (1981).
- <sup>21</sup>S. Bhakay-Tamhane and A. Sequeira, *Ferroelectrics* **69**, 241 (1986).
- <sup>22</sup>A. J. Oliveira, F. A. Germano, J. Mendes-Fihlo, F. E. A. Melo, and J. E. Moreira, *Phys. Rev. B* **38**, 12 633 (1988).
- <sup>23</sup>Y. Shiroishi, A. Nakata, and S. Sawada, *J. Phys. Soc. Jpn.* **40**, 911 (1976).
- <sup>24</sup>H. Mashiyama, K. Hasebe, S. Tanisaki, Y. Shiroishi, and S. Sawada, *J. Phys. Soc. Jpn.* **47**, 1198 (1979).
- <sup>25</sup>A. Kunishige and H. Mashiyama, *J. Phys. Soc. Jpn.* **56**, 3189 (1987).
- <sup>26</sup>H. Mashiyama, K. Hasebe, S. Tanisaki, Y. Shiroishi, and S. Sawada, *J. Phys. Soc. Jpn.* **46**, 1959 (1979).
- <sup>27</sup>A. Pietrasko, P. E. Tomaszewski, and K. Lukaszewicz, *Phase Trans.* **2**, 141 (1981).
- <sup>28</sup>K. S. Aleksandrov, L. I. Zhrebtaova, I. M. Iskornev, A. I. Kruglik, O. N. Rozanov, and I. N. Flerov, *Sov. Phys. Solid State* **22**, 2150 (1980).
- <sup>29</sup>A. I. Kruglik, M. Simonov, E. Zhelezin, and N. Belov, *Sov. Phys. Dokl.* **24**, 596 (1979).
- <sup>30</sup>T. Asahi and K. Hasebe, *J. Phys. Soc. Jpn.* **57**, 4184 (1988).
- <sup>31</sup>M. A. Pimenta, S. L. A. Vieira, F. O. V. Letelier, N. L. Speziali, and M. S. Dantas, *Solid State Commun.* **82**, 755 (1992).
- <sup>32</sup>R. Loudon, *Adv. Phys.* **13**, 423 (1964).
- <sup>33</sup>U. A. Leitão, A. Righi, P. Bourson, and M. A. Pimenta, *Phys. Rev. B* **50**, 2754 (1994).
- <sup>34</sup>D. Teeters and R. Frech, *Phys. Rev. B* **26**, 4132 (1982).
- <sup>35</sup>J. Mendes-Filho, J. E. Moreira, F. E. A. Melo, F. A. Germano, and A. S. B. Sombra, *Solid State Commun.* **60**, 189 (1986).
- <sup>36</sup>B. Kihal, C. Dugautier, and R. Farhi, *Solid State Commun.* **62**, 373 (1987).
- <sup>37</sup>B. Chary Raghunatha, H. L. Bhat, P. Chandrasekhar, and P. S. Narayanan, *J. Raman Spectrosc.* **17**, 59 (1986).
- <sup>38</sup>R. Farhi and F. Coudin, *J. Phys.: Condens. Matter* **1**, 6951 (1989).
- <sup>39</sup>A. Désert, A. Gibaud, A. Righi, U. A. Leitão, and R. L. Moreira (unpublished).